Electrocatalytic CO_2 reduction to C_{2+} products on Cu and Cu_xZn_y electrodes: Effects of chemical composition and surface morphology

Alisson H.M. da Silva [a,b], Stefan J. Raaijman [a], Cássia S. Santana [a,b], José M. Assaf [b], Janaina F. Gomes [b], Marc T.M. Koper [a,*]

[a] Leiden Institute of Chemistry, Leiden University, Leiden, Netherlands
[b] Chemical Engineering Department, São Carlos Federal University, São Carlos, São Paulo, Brazil

ARTICLE INFO

ABSTRACT

The electrocatalytic CO_2 reduction reaction (CO_2RR) is a promising strategy for producing multi-carbon compounds using only CO_2 and H_2O at room temperature. Significant advances have already been achieved in understanding how some characteristics of copper electrodes, the current state-of-the-art catalyst for multi-carbon formation via CO_2RR, affect the product spectrum. Advances and insights have been reported for, among others, the effect of crystallographic orientation, active surface area, and composition of M-copper (M = Au, Ag, Zn, etc.) materials, and how these alter the distribution of CO_2RR products. However, a systematic study evaluating the significance of these variables in the CO_2RR to C_{2+} products is still lacking in the literature and represents an important step in the development of new materials with optimized properties that can be more selective to C_{2+} compounds. In this paper, we have systematically investigated the effect of the roughness factor, chemical composition, and surface morphology of Cu_xZn_y electrocatalysts on the product distribution during CO_2RR. Firstly, Cu, $Cu_{90}Zn_{10}$, and $Cu_{75}Zn_{25}$ electrodes were exposed to oxidation-reduction cycles to produce Cu and Cu_xZn_y electrodes with different morphologies, roughness factors, and chemical composition. Our results show that an increase in the roughness factor and Zn content lead to higher faradaic efficiency (FE) to C_{2+} products. Furthermore, the influence of the nanoscale morphology is imperative for the production of C_{2+} compounds. Specifically, nanocubes of Cu and Cu_xZn_y presented the highest FE to C_{2+} products among the different surface morphologies studied in this work (polished flat surface, nanoseres, nanocubes, nanodendrites, and nanocauliflowers), showing that CC coupling during CO_2RR is mainly shape dependent.

1. Introduction

The conversion of CO_2 to molecules with high energy density via the electroreduction of CO_2 represents a promising strategy for storing renewable energy and electricity, and generating important fuels and chemicals such as hydrocarbons and alcohols from CO_2 and H_2O at ambient conditions. Many products can be obtained from the CO_2RR, such as carbon monoxide, methane, formic acid, as well as multi-carbon (C_{2+}) compounds, such as ethylene, ethanol, and propanol, which exhibit higher energy densities and higher economic value than C_1 products. Among the investigated electrodes applied to CO_2RR, copper (Cu) has been reported to be the only catalyst that has shown a significant propensity for CC coupling, leading to appreciable amounts of C_{2+} products [1].

As such, the copper-catalyzed CO_2 reduction has received much scientific interest and many advances have been made in understanding how certain characteristics of copper electrodes alter the distribution of products obtained from CO_2RR [1,2]. For example, it is known that the surface faceting affects the products distribution of the CO_2RR. Specifically,

among the three low-index Cu single crystals, the Cu(100) surface favors the formation of C_{2+} compounds over C_1, whereas the opposite is observed on Cu(110) and Cu(111) surfaces [3–5]. This knowledge has been applied in practice via the development of catalysts with controlled shapes, exposing predominantly a specific type of facet. In this direction, Wang et al. [6], for example, showed that {100}-rich Cu nanocubes yield 50% FE to C_2H_4 at −0.8 V vs. reversible hydrogen electrode (RHE), in 10 M KOH electrolyte during CO_2RR, in contrast with polycrystalline Cu nanospheres, which produce ethylene with only ∼20% of FE under the same reaction conditions. Loiudice et al. [7] showed that in addition to the geometrical effects (cubes vs. spheres), the size of the Cu cubes also has an important effect on the selectivity of C_{2+} products. They showed that cubes with 44 nm of edges results in higher FE for ethylene than cubes with 24 and 63 nm of edges. The authors suggest that the unique reactivity of the 44 nm cubes derives from an optimal balance between plane and edge sites.

Another criterion for selectivity towards C_{2+} compounds is the electrode surface area, and the associated roughness, defects, electrode potential, and current density. By increasing the amount of catalytically active

---

* Corresponding author.
  E-mail address: m.koper@lic.leidenuniv.nl. (M.T.M. Koper).

sites per geometric unit of area, i.e. the roughness factor (RF), the catalytic conversion to C_{2+} products from CO_2RR can be enhanced compared to that less roughened electrodes [8–11]. Higher roughness creates more undercoordinated sites on the electrode surface and these defects have a higher binding energy for CO_2 and/or precursor to C_{2+} compounds [11–14]. Jiang et. al [11], showed that roughened surfaces contain square sites similar to those on a Cu(100) surface but with neighboring step sites, which exhibit a favorable values of binding energy of $OC - COH$, a key precursor to C_{2+} products. Finally, rough electrodes enhance the current density which affect the selectivity of CO_2RR by changes in the local pH and/or the CO_2 mass transport. The increase in the local pH has been shown to suppress the hydrogen evolution reaction (HER) by shifting the equilibrium potential to more negative values on an SHE scale and favors CC bond formation, resulting in enhanced selectivity towards CO_2RR in general, with more multi-carbon products at lower overpotentials [2,9,15]. However, it has been shown that high current densities (> 20 mA.cm^{-2}) limits the mass transport of CO_2 to the electrode due its poor solubility in aqueous electrolytes (~34 mM at 25 °C) and hence reducing the selectivity to CO_2RR products [16]. For example, Raciti et al. [9] showed that, at -0.8 V vs. RHE in 0.1 M KHCO₃, an increase in the Cu surface roughness augmented the local pH from 9.0 to 11.0 when the RF was increased from 23 to 365. The latter, rougher, catalyst exhibited higher CO_2 conversion rates and higher FEs for C_2 compounds at low overpotentials (> -0.8 V) as compared to the catalyst with lower RF. At higher overpotentials (E ≤ -0.8 V), the local pH for the electrode with RF = 365 was even higher (reaching around 12.5 at -1.0 V), but the FE for the formation of C_{2+} compounds decreased due to the mass transport limitation of CO_2 [9].

In addition to the surface crystallographic orientation and roughness, the exact surface chemical composition of copper-based electrodes also influences the selectivity during the CO_2RR. Bimetallic copper electrodes (copper with e.g., Au, Ag or Zn) are known to promote the formation of C_{2+} compounds [8,17–19] due to a synergetic effect between the two metals. Specifically, it has been hypothesized that the dimerization of *CO (yielding *OCCO) [20–22] is enhanced on bimetallic Cu surfaces, due to an increase in θ_{CO}, because of the enhanced reduction of CO_2 to CO by Au, Ag, or Zn sites [8,17,18]. For example, Morales-Guio et al. [8] showed that, at -0.7 V vs. RHE, using 0.1 M KHCO₃ as electrolyte, a AuCu bimetallic catalyst can be two orders of magnitude more selective for CC coupled products than pristine Cu. In another study, Huang et al. [18] investigated AgCu bimetallic materials and observed that, at -1.1 V vs. RHE, using 0.1 M KHCO₃ as electrolyte, the FE to C_2H_4 increased from 13% to 37% when comparing a pure Cu catalyst with a Ag_1-$Cu_{1.1}$ bimetallic catalyst (atomic composition). In a similar study, Feng et al. [17] reported that the FE to C_2H_4 increased from 15% to 33% for a Cu and a Cu_4Zn_1 alloy (atomic composition) catalyst, respectively. In these three works, it was shown that gold, silver, or zinc generate an increased CO concentration near the surface, where copper sites then reduce it further to C_{2+} compounds. The interatomic distance is also reported to influence the selectivity during the CO_2RR. Recently, Timoshenko et. al [23] showed by in situ EXAFS that the product distribution from CO_2RR is composition- and structure-dependent: CuZn nanoparticles with shorter interatomic distance favor the production of CH_4, while nanoparticles with longer CuZn distances favor the production of CO, which is then reduced further to C_{2+}.

Although it is already known that the surface crystal orientation, roughness, and chemical composition independently can alter product distribution, a systematic study evaluating the significance of each one of these variables in conjunction to the catalytic performance of Cu-based materials in the CO_2RR to C_{2+} products is still lacking in the literature and would represent an important step in the development of new materials optimized for activity and selectivity to C_{2+} compounds. Here we explore the faradaic efficiency of the CO_2RR to C_{2+} products, investigating the concerted effects of surface roughness and nanoscale morphology on monometallic Cu and bimetallic Cu_xZn_y electrodes. The measurements provide us with insights as to which is most important characteristic for the synthesis of C_{2+} compounds: nanoparticle shape/surface morphology, chemical composition, or surface roughness.

2. Experimental section

2.1. Chemicals

KHCO₃ (99.95%, Aldrich), KCl (>99%, Aldrich), HClO₄ (60%, Aldrich), and ultrapure water (MilliQ gradient, $\geq$ 18.2 MΩcm, TOC < 5 ppb) were used as received to prepare the electrolytic solutions. CO_2 (4.5 purity, Linde) and Ar (6.0 purity, Linde) were used to saturate and purge the electrolyte.

2.2. Electrochemistry

Electrochemical cells used during experiments (standard two compartment glass cells and a custom H-cell made from PEEK) were initially cleaned by storing in acidic (0.5 M H₂SO₄, 95–98%, Sigma Aldrich) permanganate (1 g L^{-1}, >99%, Sigma Aldrich) solution overnight. Then, traces of KMnO₄ and manganese oxide were removed from the glassware and H-Cell by initial rinsing with Milli-Q water and subsequently submerging them in a solution of 10 mL L^{-1} of H₂O₂ (30% (w/w), Aldrich) and 2 mL L^{-1} of concentrated H₂SO₄ (95–98%, Aldrich) followed by boiling four times in ultrapure water (Milli-Q, $\geq$18 MΩ).

The polycrystalline Cu disk working electrode (WE) (99.99%, trace metals basis, Mateck), with a diameter of 1 cm was polished with two different alumina suspension (5 μm and 1 μm, Buehler), rinsed with ultrapure water in-between, and electropolished in a solution of 66% of H₃PO₄ by applying $+3$ V vs. a Cu counter electrode (CE) for 10 s and subsequently rinsed with ultrapure water, prior to each experiment. The $Cu_{90}Zn_{10}$ and $Cu_{75}Zn_{25}$ (99.99%, trace metals basis, Goodfellow) alloy disk electrodes (subscripts represent the atomic composition), with a diameter of 0.5 cm were similarly polished with two different alumina suspension (5 μm and 1 μm) followed by rinsing with ultrapure water, prior to each experiment.

2.3. Preparation of electrodes with different shapes

The preparation of surfaces with controlled morphology was performed according to the procedure described by Roberts, Kuhl and Nilsson [24] with some modifications. Briefly, in a 3-electrode cell with Pt wire as counter electrode and a Ag/AgCl/KCl$_{sat.}$ reference electrode, the working-electrode (Cu, $Cu_{90}Zn_{10}$, or $Cu_{75}Zn_{25}$) was subjected to 4 potential oxidation-reduction cycles in 0.1 M KHCO₃ solution containing 4 mM KCl saturated with CO_2 at a scan rate of 5 mV s^{-1} in the potential range 0.0 V ➔ E_{upper} ➔ -1.2 V vs. RHE (with E_{upper} = 0.7, 0.9 or 1.1 V vs. RHE) to synthesize surfaces with controlled morphology, specifically: irregularly shaped rounded particles (for Cu and Cu_xZn_y), called here nanospheres, nanocubes (for Cu and Cu_xZn_y), nanodendrites (for Cu) or nanocauliflowers (for Cu_xZn_y), respectively. During all electrochemical measurements, a CO_2 flow was maintained over the electrolyte to avoid ambient oxygen. The pH of the bulk CO_2-saturated electrolyte was 6.8, as measured with a pH meter. Through the oxidative treatment described above, a set of nine electrodes was obtained, denoted herein as: $Cu_{(spheres)}$, $Cu_{(cubes)}$, $Cu_{(dendrites)}$, $Cu_{90}Zn_{10(spheres)}$, $Cu_{90}Zn_{10(cubes)}$, $Cu_{90}Zn_{10(cauliflowers)}$, $Cu_{75}Zn_{25(spheres)}$, $Cu_{75}Zn_{25(cubes)}$, and $Cu_{75}Zn_{25(cauliflowers)}$.

2.4. Characterization of morphology and chemical composition

Micrographs of Cu and Cu_xZn_y electrodes (before and after oxidation-reduction cycles) were obtained by scanning electron microscopy (SEM) in an Apreo SEM (ThermoFisher Scientific) with an acceleration voltage of 15 kV and an electron beam current of 0.4 nA. Electrode chemical composition was investigated by energy dispersive X-Ray spectrometry (EDX) using an Oxford Instruments X-MaxN 150 Silicon Drift detector coupled to the Apreo SEM. EDX data processing was carried out with the Pathfinder™ X-ray Microanalysis software v1.3. The quantification of chemical elements was performed in automatic mode and the resulting electrodes chemical composition was determined by averaging the chemical compositions of at least 10 different regions of the electrode surface.

2.5. Roughness factor (RF) measurement

Electrochemically active surface area (ECSA) of the different electrodes were measured via a procedure described by Kanan and co-workers [25–27]. The experiments were carried out in a 3-electrode cell containing 0.1 M $HClO_4$. Argon was bubbled into the electrolyte for at least 15 min to remove oxygen from the solution, and a flow of argon was maintained over the solution during the electrochemical measurements. Typically, cyclic voltammetry was performed in a potential range from -0.05 V to -0.35 V vs. RHE (DL region), applying 6 different scan rates (100, 80, 60, 40, 20, and 10 mV s^{-1}). Then, the double layer capacitance was determined by plotting the DL current (in terms of geometric area) as a function of scan rate and calculating the slope of the resulting line. Assuming that the double layer capacitance value in the double layer region is proportional to the number of electrochemically active sites, it is possible to estimate the roughness factors (RF) of the electrodes by normalizing the measured capacitances with respect to that of the flat polycrystalline Cu electrode, which is conventionally taken as a reference with RF = 1.

2.6. Electrolysis experiments

CO_2 electroreduction was performed using a homemade H-cell in PEEK containing 10 mL of 0.1 M $KHCO_3$ of electrolyte per compartment. CO_2 was continuously fed at a flow rate of 10 mL min^{-1} during electrolysis. An anionic exchange membrane (AHO, AGC Inc.) was used to separate the working-electrode compartment from that of the counter-electrode. A dimensionally stable anode (DSA, Magneto) and Ag/AgCl/KCl$_{sat.}$ were used as a counter-electrode and reference electrode, respectively. All potentials measured against the Ag/AgCl/KCl$_{sat.}$ electrode were converted to RHE values according to the equation:

$$E_{RHE} = E_{Ag/AgCl(KClsat.)} + E\,^{\circ}{}_{Ag/AgCl(KClsat.)} + 0.059 \times pH$$

where E_{RHE} is the converted potential vs. RHE, $E_{Ag/AgCl(KClsat.)}$ is the experimentally measured potential against the Ag/AgCl$_{KClsat.}$ reference electrode, and $E^{\circ}{}_{Ag/AgCl(KClsat.)}$ is the standard potential of Ag/AgCl at 25 °C (0.197 V vs. NHE). Unless otherwise specified, all reported potentials herein are vs. RHE.

The potential of the working-electrode was controlled by a Biologic SP-300 potentiostat. Gaseous products were analyzed online using a Shimadzu 2014 gas chromatograph with two detectors (one TCD and one FID). Liquid products were measured by high performance liquid chromatography (HPLC) and by hydrogen nuclear magnetic resonance spectroscopy (H^1-NMR), as described elsewhere [28,29].

3. Results and discussion

The electro oxidation-reduction treatment of the Cu, $Cu_{90}Zn_{10}$ and $Cu_{75}Zn_{25}$ electrodes surfaces in presence of Cl^- to produce different surfaces exposes intricate nanostructures with controlled shapes, as depicted in Scheme 1. Fig. S1 shows the cyclic voltammograms recorded for the nine electrodes after the electro oxidation-reduction treatment. These materials are generally referred to as oxide-derived electrodes (OD-electrodes), as they are metallic electrodes resulting from the reduction of an oxide [30]. Our results show that by sweeping the potential from 0.0 V to 0.7 V vs. RHE and sweeping back from 0.7 V to -1.2 V vs. RHE (for four times), nanoparticles with irregular spherical shapes were formed on the Cu, $Cu_{90}Zn_{10}$ and $Cu_{75}Zn_{25}$ electrodes (Fig. 1a, d, and g, respectively). When the same procedure was used with an increased upper potential of 0.9 V vs. RHE, nanocubes with 54 ± 5 nm of edge size were formed for Cu and both Cu_xZn_y electrodes (Fig. 1b, e, and h, respectively). In agreement with previous work, we consider these images as evidence for (100) facets [24,31–33]. It is known that copper nanocubes can be synthesized via this procedure [24,31–33], but we report here the applicability of this method for synthesizing Cu_xZn_y nanocubes. Lastly, when the oxidation potential was increased to 1.1 V, Cu nanodendrites (Fig. 1c), looking like double compound leaves, or Cu_xZn_y "nanocauliflowers" (Fig. 1f and i) were formed instead. SEM images of the Cu, $Cu_{90}Zn_{10}$, and $Cu_{75}Zn_{25}$ electrodes before the oxidation-reduction treatment are shown in Fig. S2.

These materials were also characterized by cyclic voltammetry in 0.1 M NaOH solution between -0.25 V to 0.45 V vs RHE [34], and the results are shown in Fig. 2. For Cu electrodes before the electro oxidation-reduction treatment (Fig. 2a), symmetrical oxidation and reduction peaks were observed at -0.15 V, 0.05 V, 0.35 V and 0.43 V vs RHE. The peaks of low intensity at -0.15 V and -0.05 V correspond to the adsorption and desorption of OH^- on Cu (100) terraces and Cu (111) terraces, respectively, and the pronounced peaks at 0.35 V and 0.43 V are both related to the oxidation and reduction of Cu to Cu_2O on different domains of the polycrystalline electrode. For the OD-Cu electrodes (Fig. 2b), the same profile was observed, but with peaks of significantly higher intensity. This increase in the current is due to an increase in surface roughness as consequence of
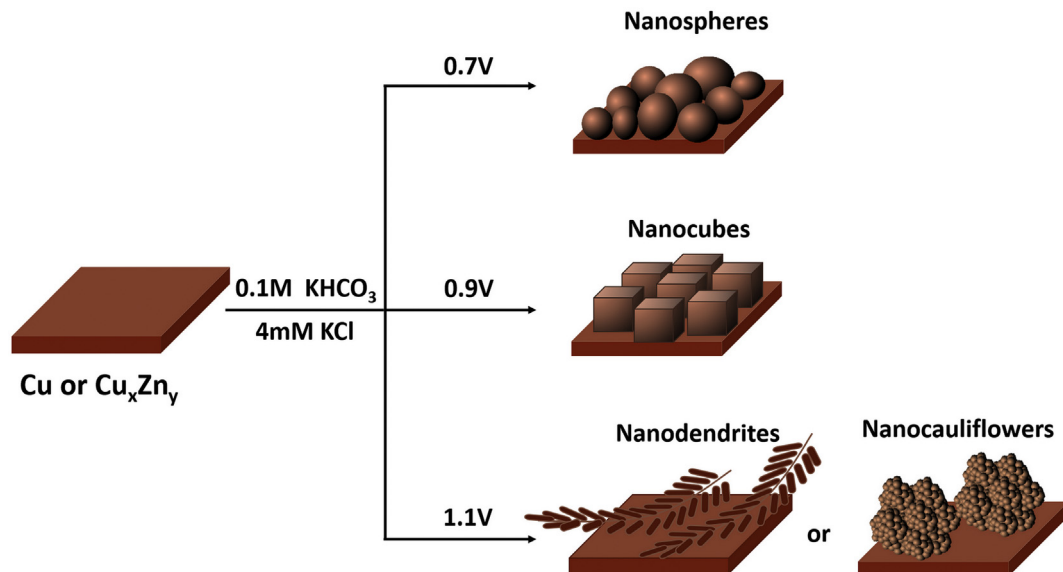
Scheme 1. Preparation of Cu, $Cu_{90}Zn_{10}$, and $Cu_{75}Zn_{25}$ electrodes which expose nanospheres, nanocubes, or nanodendrites/nanocauliflowers by cycling from -1.2 V vs RHE to 0.7 V, 0.9 V, or 1.1 V vs. RHE, respectively. Electrolyte: 0.1 M $KHCO_3$ + 4 mM KCl.
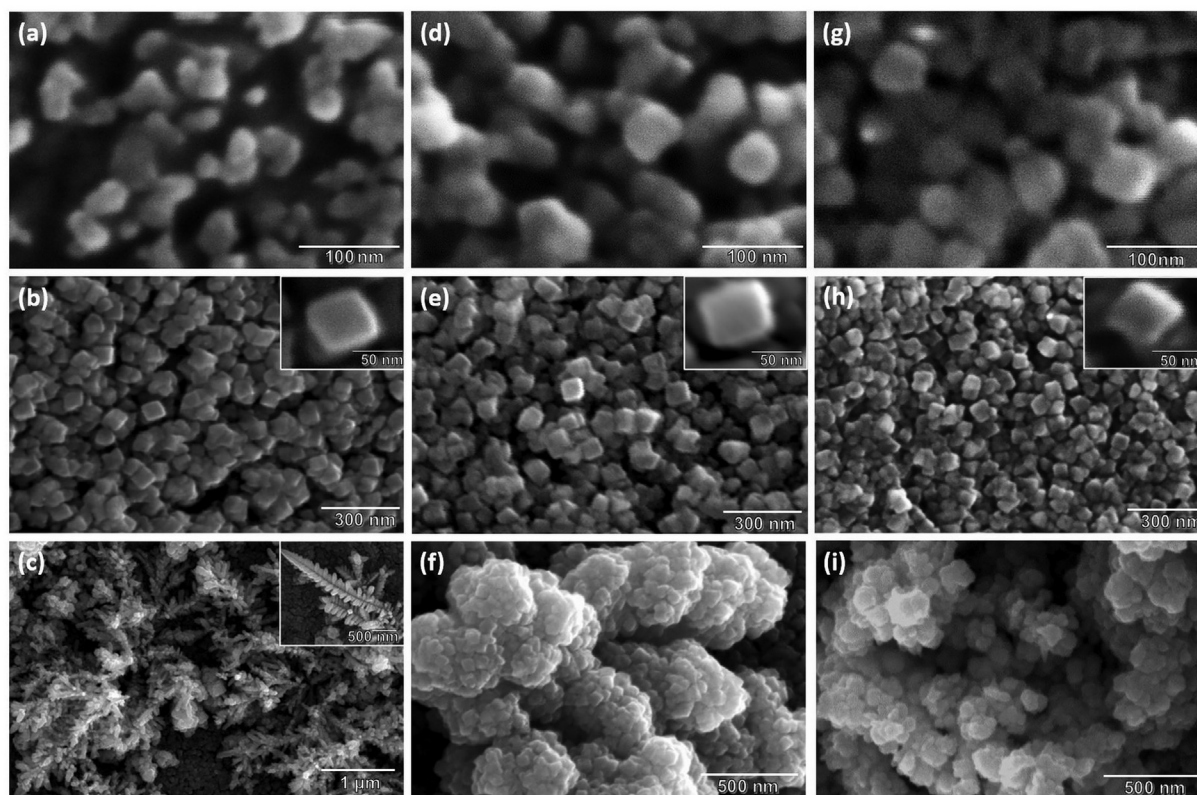
Fig. 1. SEM images of (a) OD-Cu$_{(spheres)}$, (b) OD-Cu$_{(cubes)}$, (c) OD-Cu$_{(dendrites)}$, (d) OD-Cu$_{90}$Zn$_{10(spheres)}$, (e) OD-Cu$_{90}$Zn$_{10(cubes)}$, (f) OD-Cu$_{90}$Zn$_{10(cauliflowers)}$, (g) OD-Cu$_{75}$Zn$_{25}$ $_{(spheres)}$, (h) OD-Cu$_{75}$Zn$_{25(cubes)}$, (i) OD-Cu$_{75}$Zn$_{25}$ $_{(cauliflowers)}$.

the oxidation-reduction treatment. The corresponding electrode surface area will be discussed in more detail when we present the results concerning the roughness factor. For CuZn electrodes before the oxidation-reduction treatment (Fig. 2c and e), significant differences between the voltammetric profiles were found, although the same procedure was used. A broad peak between -0.2 V and -0.05 V was observed for the Cu$_{90}$Zn$_{10}$ electrode (Fig. 2c) and it became more pronounced for samples with increased zinc content, e.g., Cu$_{75}$Zn$_{25}$ (Fig. 2e), suggesting that these voltammetric features are related to Zn. For OD-CuZn electrodes (Fig. 2d and f) an increase in the current was also observed, as observed for OD-Cu, with intense voltammetric features between -0.3 V $\leq$ E $\leq$ 0.45 V, indicative of increased surface area after the oxidation-reduction treatment. The appearance of the oxidation-reduction peaks between 0.0 and 0.1 V suggests that cycling the CuZn electrodes exposes more Cu to the surface. The electrochemical characterization was mainly used here as a reference: Cu, OD-Cu, CuZn, and OD-CuZn were systematically prepared and characterized in NaOH prior to being subjected to the CO$_2$RR conditions, ensuring reproducible surface conditions at the beginning of each measurement.

The atomic composition of the electrodes at the surface before and after the oxidation-reduction treatment was investigated by SEM-EDX and the results are shown in Table 1. For the Cu electrodes, only copper was identified on the surface, as expected. For the Cu$_{90}$Zn$_{10}$ and Cu$_{75}$Zn$_{25}$ alloys, before the oxidation-reduction treatment, the contents of Cu and Zn on the surfaces were close to those reported by the supplier. Specifically, a composition of 88.2 $\pm$ 5.2% of Cu and 11.1 $\pm$ 2.4% of Zn was found for Cu$_{90}$Zn$_{10}$ and 73.2 $\pm$ 4.8% of Cu and 24.6 $\pm$ 2.1% of Zn for Cu$_{75}$Zn$_{25}$. However, after the oxidation-reduction, the atomic composition of the surface for zinc-containing bimetallic catalysts changed in comparison to their composition before the treatment. Particularly, the relative content of zinc at the surface gradually decreased as the oxidation potential in the oxidation-reduction procedure was increased. For example, for the Cu$_{75}$Zn$_{25(spheres)}$ electrode, which was subjected to a maximum of 0.7 V, the surface atomic composition was found to be 79.1 $\pm$ 5.1% of Cu and 21.7 $\pm$ 2.9% of Zn, as compared to

the original value of 73.2 $\pm$ 4.8% of Cu and 24.6 $\pm$ 2.1% of Zn. For the Cu$_{75}$Zn$_{25(cubes)}$ electrode, oxidized up to 0.9 V, only 13.6 $\pm$ 2.7% of Zn was found and for the Cu$_{75}$Zn$_{25(cauliflowers)}$, oxidized up to 1.1 V, the Zn content was again lower, measuring only 6.1 $\pm$ 1.6% at the surface. The same trend was observed for the Cu$_{90}$Zn$_{10}$ electrodes. The decrease of Zn content at the surface can be explained by the electrodissolution of zinc into the electrolyte, as Zn can easily be oxidized to Zn^{+2} at potentials positive of the equilibrium potential (Zn $\leftrightarrow$ Zn^{2+} + 2e$^-$, E° (V) = -0.3606 V vs. RHE at pH = 6.8). As the equilibrium potential for zinc lies well below that of copper, this can reasonably explain the relative enrichment of the surface in copper as the driving force for the leaching of zinc is relatively greater, with increased upper oxidation limits enhancing this effect. Our results therefore show that, by applying the oxidation-reduction procedure, not only the surface morphology is modified, but also the chemical composition at the interface.

Surface roughness factors (RF) of the Cu and Cu$_x$Zn$_y$ electrodes were determined through measurement of the double layer (DL) capacitance by recording cyclic voltammograms in the double layer window, and the results are shown in Table 1 (RFs) and Fig. S3 (DL current measurements and analysis). For the OD-Cu and OD-Cu$_x$Zn$_y$ electrodes, higher capacitance and hence higher roughness factor values were obtained when the final oxidation potential was increased in the oxidation-reduction treatment. For example, Cu$_{(dendrites)}$, which were cycled up to 1.1 V vs. RHE, presented a higher roughness factor (RF = 5.5) than Cu$_{(cubes)}$ (RF = 2.9), which formed upon cycling to 0.9 V vs. RHE, which was still higher than the roughness of an uncycled polished copper surface (RF = 1). This increase in the roughness factor by applying increasingly positive oxidation potentials during electrochemical cycling can be explained by higher surface disorder upon reduction of the increasingly thicker copper oxide layer. Specifically, when Cu electrodes are used, Cl$^-$ reacts with Cu to form CuCl. At oxidative potentials at neutral or basic pH, CuCl is converted to Cu$_2$O through two reactions in series (CuCl + OH$^-$ $\leftrightarrow$ CuOH + Cl$^-$ and 2CuOH $\leftrightarrow$ Cu$_2$O + H$_2$O) [24,35,36]. By cycling to increasingly positive potentials, thicker oxide layers are generated which result in more disordered surfaces
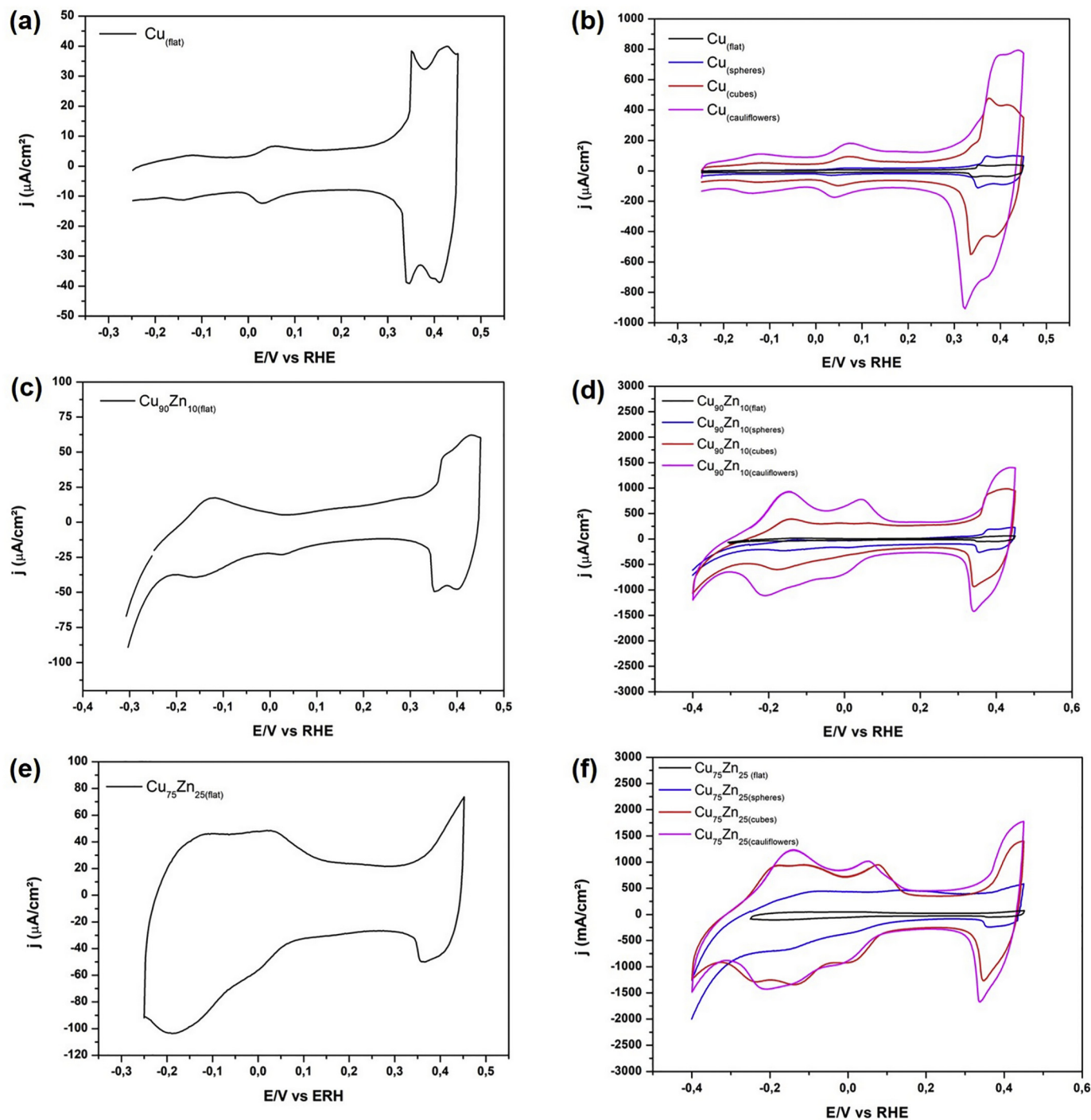
Fig. 2. Cyclic voltammograms of (a) $Cu_{(flat)}$; (b) OD-Cu; (c) $Cu_{90}Zn_{10(flat)}$; (d) OD-$Cu_{90}Zn_{10}$; (e) $Cu_{75}Zn_{25(flat)}$; and (f) OD-$Cu_{75}Zn_{25}$ electrodes in 0.1 M NaOH at a scan rate of 50 mV s^{-1}.

upon reduction and hence in progressively higher surface roughness values as one cycles to more oxidative potentials.

CO_2 electroreduction in CO_2-saturated 0.1 M $KHCO_3$ (pH = 6.8) was performed at four different potentials (-0.8, -0.9, -1.0, and -1.1 V vs RHE) on Cu and Cu_xZn_y electrodes. It is important to point out that in the oxidation-reduction treatment over the electrodes, the sweeping of the potential ends at -1.2 V vs. RHE and thus it is considered that the Zn and Cu are both in metallic form. In addition, we note that Chen et al. [33] showed by HR-TEM that the morphology of the nanoparticles remained as cubes even after 70 min of CO_2 electroreduction in CO_2-saturated 0.1 M $KHCO_3$, pH = 6.8 (same reaction conditions as applied

in our experiments). Furthermore, they also showed the presence of (100) facets in their HR-TEM images reinforcing the stability of the particles under the applied reaction conditions. The corresponding faradaic efficiencies to H_2, CO, CH_4, HCOOH, C_2H_4, EtOH, and PrOH (main products identified herein) are shown in Table S1. The sum of FE varied from 85%, for the lowest potentials, to 105%, for the highest potentials. As small amounts of aldehydes, ketones, and other liquid products have not been quantified and they are preferably formed at lower potentials, the total FE at -0.8 and -0.9 V vs RHE is below 90%. For the higher potentials, only gaseous products and higher alcohols are preferably formed and thus it is reasonable to achieve total FE close to 100% since they were all quantified. Values

Table 1
Atomic composition, as studied by SEM-EDS, and roughness factor of the Cu, OD-Cu, Cu$_{90}$Zn$_{10}$, OD-Cu$_{90}$Zn$_{10}$, Cu$_{75}$Zn$_{25}$ and OD-Cu$_{75}$Zn$_{25}$ electrodes.

Sample	Atomic composition (by EDS)		Roughness factor (compared to Cu$_{(flat)}$)
	Cu (%)	Zn (%)	
Cu$_{(flat)}$	100	0	1.0
OD-Cu$_{(spheres)}$	100	0	1.8
OD-Cu$_{(cubes)}$	100	0	2.9
OD-Cu$_{(dendrites)}$	100	0	5.5
Cu$_{90}$Zn$_{10(flat)}$	88.2 ± 5.2	11.1 ± 2.4	2.7
OD-Cu$_{90}$Zn$_{10(spheres)}$	91.4 ± 4.9	8.6 ± 2.0	5.1
OD-Cu$_{90}$Zn$_{10(cubes)}$	93.1 ± 4.3	6.8 ± 2.0	12.9
OD-Cu$_{90}$Zn$_{10(cauliflowers)}$	97.4 ± 4.7	2.8 ± 1.5	18.8
Cu$_{75}$Zn$_{25(flat)}$	73.2 ± 4.8	24.6 ± 2.1	7.1
OD-Cu$_{75}$Zn$_{25(spheres)}$	79.1 ± 5.1	21.7 ± 2.9	7.4
OD-Cu$_{75}$Zn$_{25(cubes)}$	86.4 ± 5.5	13.6 ± 2.7	15.0
OD-Cu$_{75}$Zn$_{25(cauliflowers)}$	95.9 ± 4.7	6.1 ± 1.6	18.2

found around 105% are due to cumulative experimental errors since different quantification techniques were used (GC, HPLC and H^1-NMR). As a general trend, with some exceptions, the faradaic efficiency (FE) of the H$_2$ and CO production decreased when a higher reduction potential was applied. For example, for the Cu$_{(cubes)}$ electrode the FE of the H$_2$ synthesis diminished from 49.3% at −0.8 V to 22.3% at −1.1 V. The same behavior was also observed for CO, for which FE decreased from 13.6% at −0.8 V to 2.6% at −1.1 V. On the other hand, for C$_{2+}$ products (C$_2$H$_4$, EtOH and PrOH), higher FEs were observed for the Cu and Cu$_x$Zn$_y$ electrodes at more reductive potentials. The opposite trends observed for CO formation and that of C$_{2+}$ compounds is consistent with the fact that adsorbed CO is the key species of the CO dimerization considered to be involved in the C$_{2+}$ synthesis [1,2,37]. At these more negative potentials, the higher current leads to more hydroxide formation and thus to an increase in local pH near the electrode. In turn, this inhibits the hydrogen evolution reaction [9,38,39] and hence favors to the formation of carbon products. In the present work, we are interested in evaluating how the catalytic performance towards the production of C$_{2+}$ compounds is affected by the surface morphology (nanoparticle shapes), the roughness factor and the composition of the interface. As the best potential for C$_{2+}$ product formation on the investigated electrodes was −1.1 V vs RHE, the following discussion will be focused on the C$_{2+}$ production at this potential.

Fig. 3 shows the FEs to C$_2$H$_4$, EtOH, and PrOH (C$_{2+}$ products identified here) for the Cu (Fig. 3a), Cu$_{90}$Zn$_{10}$ (Fig. 3b), and Cu$_{75}$Zn$_{25}$ (Fig. 3c) electrodes at −1.1 V, before and after the oxidation-reduction treatment. The values of the RF were added below the name of each electrode to make the discussion easier, since the increase in the RF is considered to be one of the important factors for improving the catalytic performance of the CO$_2$ reduction [2,9,15,16]. For the electrodes without the oxidation-reduction treatment (polished flat electrodes), the faradaic efficiency to C$_{2+}$ compounds were around 15% for Cu and Cu$_{90}$Zn$_{10}$ and decreased to about 7.5% for the Cu$_{75}$Zn$_{25}$ electrode. This result shows that the mere addition of Zn to the Cu structure does not enhance the C$_{2+}$ production. By contrast, C$_{2+}$ production decreases when the atomic percentage of Zn in the electrode increases from ca. 10% to approximately 25%, even though the roughness factor increased from 1.0 for Cu to 7.1 for the Cu$_{75}$Zn$_{25}$ alloy. Instead of C$_{2+}$ production, CH$_4$ and H$_2$ are enhanced by Cu$_{90}$Zn$_{10}$ and Cu$_{75}$Zn$_{25}$, respectively (Table S1). This behavior agrees with the results of Timoshenko et. al [23], who showed that CH$_4$, H$_2$, and CO production were dependent of the composition and structure of CuZn and specifically that a low content of Zn leads to higher CH$_4$ formation and high content of Zn leads to higher H$_2$ formation as observed here for Cu$_{90}$Zn$_{10}$ and Cu$_{75}$Zn$_{25}$. On the other hand, our results differs from results reported by Feng et al. [17] who showed that CuZn alloy can enhance the C$_{2+}$ production in comparison to the pure Cu. However, in that work the authors synthesized spherical nanoparticles of CuZnO alloys with 7 to 15 nm in diameter by pulsed laser ablation of a CuZn alloy target and, before the

CO$_2$RR tests, CuZnO alloys were deposited on glassy carbon and reduced at −1.6 V vs RHE, producing OD-electrodes. Therefore, in the studies reported by Feng et al. [17] not only the composition effect (Cu$_x$Zn$_y$ vs Cu) was considered, but also the influence of the nanoparticle size, dispersion, subsurface oxygen, etc. Here, by investigating non-oxidized Cu, Cu$_{90}$Zn$_{10}$, and Cu$_{75}$Zn$_{25}$ polished disc electrodes with low surface roughness, morphological and/or particle size effects and surface roughness effects between the different electrodes were minimized leading to more accurate relationships between the Zn content in the CuZn alloy and the catalytic performance of the electrodes towards the formation of C$_{2+}$ compounds.

For the electrodes obtained after oxidation-reduction treatment (OD-electrodes), catalytic performances were significantly improved in comparison to the flat Cu and Cu$_x$Zn$_y$ electrodes. The catalytic behavior is similar for the OD-Cu, OD-Cu$_{90}$Zn$_{10}$, and OD-Cu$_{75}$Zn$_{25}$ electrodes. Specifically, the faradaic efficiency towards C$_{2+}$ products increases going from a polished flat surface to a nanosphere-covered electrode, reaching the highest performance for surfaces comprised of nanocubes, and decreasing in the case of nanodendrite (for Cu) or nanocauliflower (for Cu$_x$Zn$_y$) morphologies. In general, the catalytic performance seems to be impacted by the surface roughness factor, chemical composition, and nanostructure shape.

To obtain a better understanding of the influence of the roughness factor, Fig. 3d shows the FE to C$_{2+}$ compounds for the oxide derived Cu, Cu$_{90}$Zn$_{10}$, and Cu$_{75}$Zn$_{25}$ electrodes containing nanocubular features. The effect of the nanoparticle shape is minimized here since the electrodes contain cubic nanostructures of similar sizes, although the chemical composition is not identical between different electrodes. It is evident that the production of C$_{2+}$ compounds is enhanced with increasing surface roughness factor, for the same type of surface morphology. The same trend was also observed for the nanosphere electrodes. Cu$_{75}$Zn$_{25(spheres)}$ has a higher RF and higher FE to C$_{2+}$ than Cu$_{90}$Zn$_{10(spheres)}$ and Cu$_{(spheres)}$. However, besides the surface roughness factor, the Zn content was also higher for the Cu$_{75}$Zn$_{25}$ nanocubes and Cu$_{75}$Zn$_{25}$ nanospheres electrodes in comparison with the Cu$_{90}$Zn$_{10}$ and pure Cu materials. Although for the polished flat electrodes, the presence of Zn in Cu is not beneficial to the C$_{2+}$ production (Fig. 3), by subjecting the Cu and Cu$_x$Zn$_y$ electrodes to electrochemical cycling, surface morphologies containing nanostructures with different size and shapes are formed and hence the physical and electronic properties of the OD-electrodes are likely different from those of the non-oxidized, mechanically polished surfaces. Therefore, in contrast to the polished flat electrodes, we cannot discard the existence of synergistic effects between Zn and Cu in the OD-electrodes and this can also contribute to improve the production of C$_{2+}$ compounds, as previously reported by other authors [17,19,40–42]. In comparison to the materials investigated by Feng et al. [17], our OD-electrodes are in better agreement regarding their electrocatalytic behavior than polished flat electrodes: we also see a higher production of C$_{2+}$ compounds on Cu$_x$Zn$_y$ alloys compared to pure Cu. Further evidence that the zinc content has a positive impact on the catalytic performance of OD-Cu$_x$Zn$_y$ electrodes towards the production of C$_{2+}$ compounds is provided by the nanocauliflower materials. For Cu$_{75}$Zn$_{25(cauliflower)}$ (%Zn = 6.1 ± 1.6) the RF is slightly lower than that of Cu$_{90}$Zn$_{10(cauliflower)}$ (% Zn = 2.8 ± 1.5), but Cu$_{75}$Zn$_{25(cauliflower)}$ presents a higher FE for C$_{2+}$ compounds (~44% for Cu$_{75}$Zn$_{25(cauliflower)}$ versus ~33% for Cu$_{90}$Zn$_{10(cauliflower)}$). Therefore, it seems that for the OD-Cu$_x$Zn$_y$ electrodes, a higher zinc content leads to improved C$_{2+}$ production.

Even though, in general, RF and Zn content can both improve the selectivity towards higher FE to C$_{2+}$ products, when comparing different nanoparticle geometries, it is clear the shape is dominant factor for the synthesis of C$_{2+}$ compounds. When we move from nanocubes to nanodendrites or nanocauliflowers, even though the roughness factor increases, the FE to C$_{2+}$ products decrease. From nanocubes to nanospheres, an increase in the Zn content is observed but also a decrease in FE to C$_{2+}$ products. In other words, whenever the structure is diverted from the nanocubes, even if the RF or Zn content are increased, the production of C$_{2+}$ compounds is reduced. Nanocubes are well-known to expose preferentially {100} facets [6,24,43] and, according to previous studies with copper single crystals
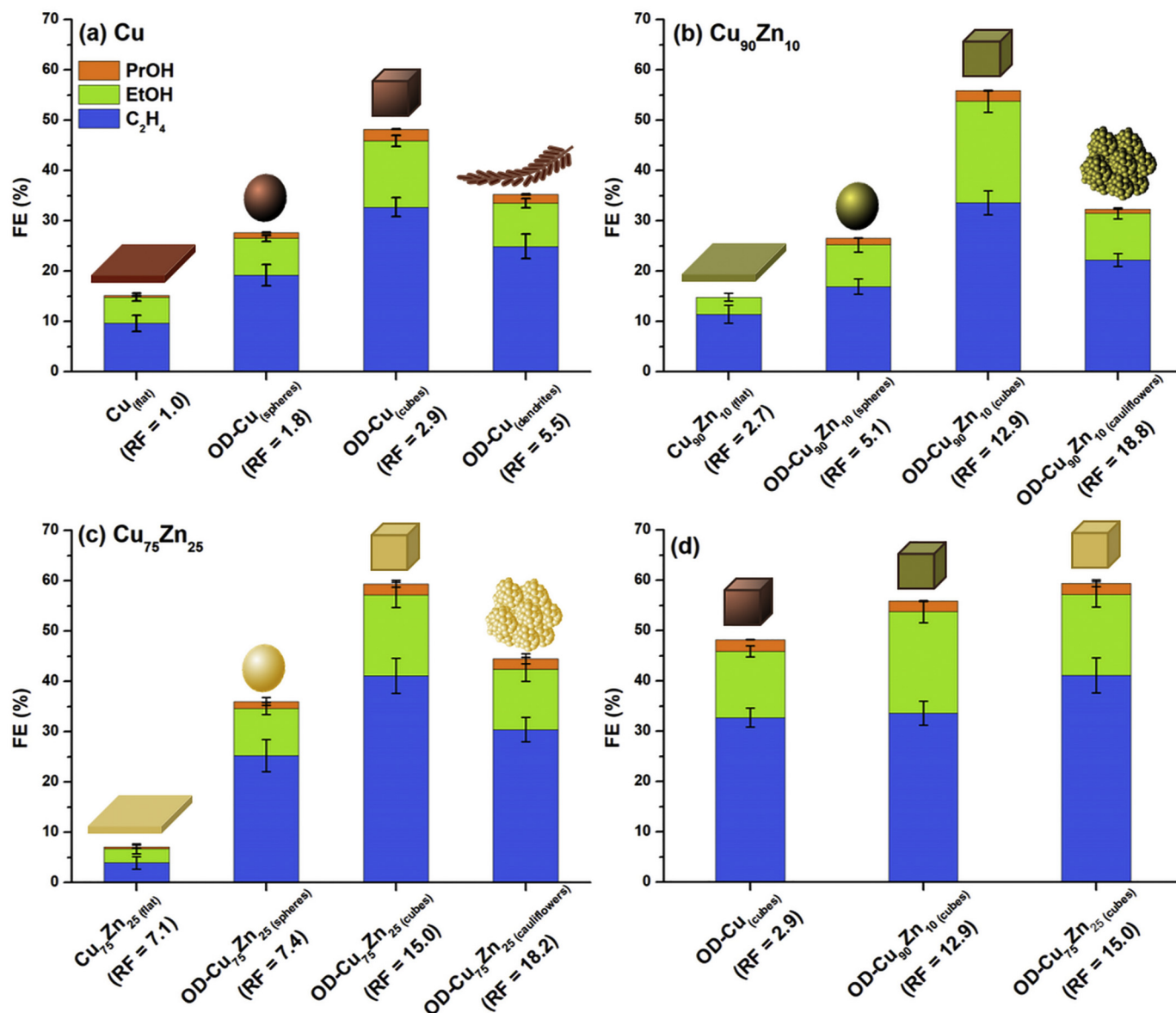
Fig. 3. Faradaic efficiency (FE) of the C_2H_4 (blue), EtOH (green), and PrOH (orange) production on (a) $Cu_{(flat)}$, OD-$Cu_{(spheres)}$, OD-$Cu_{(cubes)}$, and OD-$Cu_{(dendrites)}$, (b) $Cu_{90}Zn_{10}$ (flat), OD-$Cu_{90}Zn_{10(spheres)}$, OD-$Cu_{90}Zn_{10(cubes)}$, and OD-$Cu_{90}Zn_{10(cauliflowers)}$, (c) $Cu_{75}Zn_{25(flat)}$, OD-$Cu_{75}Zn_{25(spheres)}$, OD-$Cu_{75}Zn_{25(cubes)}$, and OD-$Cu_{75}Zn_{25(cauliflowers)}$, and (d) OD-$Cu_{(cubes)}$, OD-$Cu_{90}Zn_{10(cubes)}$, and OD-$Cu_{75}Zn_{25(cubes)}$ at -1.1 V vs RHE. Roughness factor (RF) values were added below the name of each electrode to facilitate the discussion.(For interpretation of the references to color in this figure legend, the reader is referred to the web version of this article.)

[1–5], C_{2+} products are favorably synthesized on Cu(100), while C_1 compounds are mainly formed on Cu(110) and Cu(111). Therefore, the best performance of nanocubes exposed-OD-electrodes for the synthesis of C_{2+} products can be associated with the preferential exposition of {100} facets. To date, relevant advances have been reported with respect to the impacts of roughness [8–11], crystalline structure [3–5], composition of CuZn electrodes [17,23,40,41], interatomic distance between Cu and Zn [23], etc., on the CO_2RR. However, here we show that among all these important characteristics, the particle geometry is a dominant factor in the synthesis of C_{2+} compounds.

4. Conclusions

Cu and Cu_xZn_y electrodes with different zinc contents, roughness factors, and surface morphologies were successfully prepared by electrocycling polished Cu, $Cu_{90}Zn_{10}$, and $Cu_{75}Zn_{25}$ electrodes between -1.2 V and 0.7 V, 0,9 V, or 1.1 V vs. RHE in 0.1 M $KHCO_3$ containing 4 mM KCl. From SEM images, it was observed that nanospheres (for Cu

and Cu_xZn_y), nanocubes (for Cu and Cu_xZn_y) and nanodendrites (for Cu) or nanocauliflowers (for Cu_xZn_y) were formed when the oxidation potential was changed from 0.7 V to 0.9 V, and 1.1 V, respectively. Surface roughness was increased when higher oxidation potential limits were applied to the electrodes during the oxidation-reduction treatment (nanocauliflowers~nanodendrites > nanocubes > nanospheres). The production of C_{2+} compounds was showed to be influenced by the roughness factor, zinc content, and nanostructure shape. For a given shape, increasing the surface roughness factor led to higher FEs to C_{2+} compounds. The increase of zinc content in the polished flat electrodes showed to decrease the amount C_{2+} compounds produced. On the other hand, for OD-electrodes of a given shape, zinc content leads to a higher total FE for C_{2+}. Although both roughness factor and catalyst alloy composition can impact the catalytic performance towards the production of C_{2+} compounds, the electrode nanostrucure shape showed to be the biggest factor in enhancing C_{2+} formation. Specifically, nanocube (which preferentially expose {100} facets) covered surfaces of Cu and Cu_xZn_y electrocatalysts, were found to lead to higher FE to C_{2+} compounds among the different shapes evaluated in this

work (nanospheres, nanocubes, nanodendrites and nanocauliflowers). We believe these results provide important guidelines for the rational design of optimized electrodes to be applied in the conversion of CO_2 to C_{2+} compounds.

Declaration of Competing Interest

Acknowledgements

Appendix A. Supplementary data

Supplementary data to this article can be found online at https://doi.org/10.1016/j.jelechem.2020.114750.

References

[1] S. Nitopi, E. Bertheussen, S.B. Scott, X. Liu, A.K. Engstfeld, S. Horch, B. Seger, I.E.L. Stephens, K. Chan, C. Hahn, J.K. Nørskov, T.F. Jaramillo, I. Chorkendorff, Progress and perspectives of electrochemical CO_2 reduction on copper in aqueous electrolyte, Chem. Rev. 119 (2019) 7610–7672, https://doi.org/10.1021/acs.chemrev.8b00705.

[2] Y.Y. Birdja, E. Pérez-Gallent, M.C. Figueiredo, A.J. Göttle, F. Calle-Vallejo, M.T.M. Koper, Advances and challenges in understanding the electrocatalytic conversion of carbon dioxide to fuels, Nat. Energy 4 (2019) 732–745, https://doi.org/10.1038/s41560-019-0450-y.

[3] K.W. Frese, Electrochemical reduction of CO_2 at solid electrodes, in: B.P. Sullivan (Ed.), Electrochem. Electrocatal. React. Carbon Dioxide, Elsevier 1993, pp. 145–213.

[4] Y. Hori, H. Wakebe, T. Tsukamoto, O. Koga, Adsorption of CO accompanied with simultaneous charge transfer on copper single crystal electrodes related with electrochemical reduction of CO_2 to hydrocarbons, Surf. Sci. 335 (1995) 258–263, https://doi.org/10.1016/0039-6028(95)00441-6.

[5] Y. Huang, A.D. Handoko, P. Hirunsit, B.S. Yeo, Electrochemical reduction of CO_2 using copper single-crystal surfaces: effects of CO* coverage on the selective formation of ethylene, ACS Catal. 7 (2017) 1749–1756, https://doi.org/10.1021/acscatal.6b03147.

[6] Y. Wang, H. Shen, K.J.T. Livi, D. Raciti, H. Zong, J. Gregg, M. Onadeko, Y. Wan, A. Watson, C. Wang, Copper nanocubes for CO_2 reduction in gas diffusion electrodes, Nano Lett. 19 (2019) 8461–8468, https://doi.org/10.1021/acs.nanolett.9b02748.

[7] A. Loiudice, P. Lobaccaro, E.A. Kamali, T. Thao, B.H. Huang, J.W. Ager, R. Buonsanti, Tailoring copper nanocrystals towards C_2 products in electrochemical CO_2 reduction, Angew. Chem. Int. Ed. 55 (2016) 5789–5792, https://doi.org/10.1002/anie.201601582.

[8] C.G. Morales-Guio, S.A. Nitopi, J.T. Feaster, L. Wang, K.P. Kuhl, A. Jackson, N.C. Johnson, D.N. Abram, T. Hatsukade, C. Hahn, T.F. Jaramillo, Improved CO_2 reduction activity towards C_{2+} alcohols on a tandem gold on copper electrocatalyst, Nat. Catal. 1 (2018) 764–771, https://doi.org/10.1038/s41929-018-0139-9.

[9] D. Raciti, M. Mao, J.H. Park, C. Wang, Local pH effect in the CO_2 reduction reaction on high-surface-area copper Electrocatalysts, J. Electrochem. Soc. 165 (2018) F799–F804, https://doi.org/10.1149/2.0521810jes.

[10] B. Qin, H. Wang, F. Peng, H. Yu, Y. Cao, Effect of the surface roughness of copper substrate on three-dimensional tin electrode for electrochemical reduction of CO_2 into HCOOH, J. CO_2 Util. 21 (2017) 219–223, https://doi.org/10.1016/j.jcou.2017.07.012.

[11] K. Jiang, Y. Huang, G. Zeng, F.M. Toma, W.A. Goddard, A.T. Bell, Effects of surface roughness on the electrochemical reduction of CO_2 over Cu, ACS Energy Lett. 5 (2020) 1206–1214, https://doi.org/10.1021/acsenergylett.0c00482.

[12] Y. Wang, P. Han, X. Lv, L. Zhang, G. Zheng, Defect and interface engineering for aqueous electrocatalytic CO_2 reduction, Joule. 2 (2018) 2551–2582, https://doi.org/10.1016/j.joule.2018.09.021.

[13] Y. Lum, B. Yue, P. Lobaccaro, A.T. Bell, J.W. Ager, Optimizing C–C coupling on oxide-derived copper catalysts for electrochemical CO_2 reduction, J. Phys. Chem. C 121 (2017) 14191–14203, https://doi.org/10.1021/acs.jpcc.7b03673.

[14] T.-T. Zhuang, Z.-Q. Liang, A. Seifitokaldani, Y. Li, P. De Luna, T. Burdyny, F. Che, F. Meng, Y. Min, R. Quintero-Bermudez, C.T. Dinh, Y. Pang, M. Zhong, B. Zhang, J. Li, P.-N. Chen, X.-L. Zheng, H. Liang, W.-N. Ge, B.-J. Ye, D. Sinton, S.-H. Yu, E.H. Sargent, Steering post-C–C coupling selectivity enables high efficiency electroreduction of carbon dioxide to multi-carbon alcohols, Nat. Catal. 1 (2018) 421–428, https://doi.org/10.1038/s41929-018-0084-7.

[15] W. Tang, A.A. Peterson, A.S. Varela, Z.P. Jovanov, L. Bech, W.J. Durand, S. Dahl, J.K. Nørskov, I. Chorkendorff, The importance of surface morphology in controlling the selectivity of polycrystalline copper for CO_2 electroreduction, Phys. Chem. Chem. Phys. 14 (2012) 76–81, https://doi.org/10.1039/C1CP22700A.

[16] D. Ren, J. Fong, B.S. Yeo, The effects of currents and potentials on the selectivities of copper toward carbon dioxide electroreduction, Nat. Commun. 9 (2018) 925, https://doi.org/10.1038/s41467-018-03286-w.

[17] Y. Feng, Z. Li, H. Liu, C. Dong, J. Wang, S.A. Kulinich, X. Du, Laser-prepared CuZn alloy catalyst for selective electrochemical reduction of CO_2 to ethylene, Langmuir. 34 (2018) 13544–13549, https://doi.org/10.1021/acs.langmuir.8b02837.

[18] J. Huang, J. Mensi, E. Oveisi, V. Mantella, R. Buonsanti, Structural sensitivities in bimetallic catalysts for electrochemical CO_2 reduction revealed by Ag–Cu nanodimers, J. Am. Chem. Soc. 141 (2019) 2490–2499, https://doi.org/10.1021/jacs.8b12381.

[19] T. Zhang, Z. Li, J. Zhang, J. Wu, Enhance CO2-to-C2+ products yield through spatial management of CO transport in Cu/ZnO tandem electrodes, J. Catal. 387 (2020) 163–169, https://doi.org/10.1016/j.jcat.2020.05.002.

[20] R. Kortlever, J. Shen, K.J.P. Schouten, F. Calle-Vallejo, M.T.M. Koper, Catalysts and reaction pathways for the electrochemical reduction of carbon dioxide, J. Phys. Chem. Lett. 6 (2015) 4073–4082, https://doi.org/10.1021/acs.jpclett.5b01559.

[21] F. Calle-Vallejo, M.T.M. Koper, Theoretical considerations on the Electroreduction of CO to C_2 species on Cu(100) electrodes, Angew. Chem. Int. Ed. 52 (2013) 7282–7285, https://doi.org/10.1002/anie.201301407.

[22] E. Pérez-Gallent, M.C. Figueiredo, F. Calle-Vallejo, M.T.M. Koper, Spectroscopic observation of a hydrogenated CO dimer intermediate during CO reduction on Cu(100) electrodes, Angew. Chem. Int. Ed. 56 (2017) 3621–3624, https://doi.org/10.1002/anie.201700580.

[23] J. Timoshenko, H.S. Jeon, I. Sinev, F.T. Haase, A. Herzog, B. Roldan Cuenya, Linking the evolution of catalytic properties and structural changes in copper–zinc nanocatalysts using operando EXAFS and neural-networks, Chem. Sci. 11 (2020) 3727–3736, https://doi.org/10.1039/D0SC00382D.

[24] F.S. Roberts, K.P. Kuhl, A. Nilsson, High selectivity for ethylene from carbon dioxide reduction over copper nanocube electrocatalysts, Angew. Chem. 127 (2015) 5268–5271, https://doi.org/10.1002/ange.201412214.

[25] A. Verdaguer-Casadevall, C.W. Li, T.P. Johansson, S.B. Scott, J.T. McKeown, M. Kumar, I.E.L. Stephens, M.W. Kanan, I. Chorkendorff, Probing the active surface sites for CO reduction on oxide-derived copper electrocatalysts, J. Am. Chem. Soc. 137 (2015) 9808–9811, https://doi.org/10.1021/jacs.5b06227.

[26] C.W. Li, J. Ciston, M.W. Kanan, Electroreduction of carbon monoxide to liquid fuel on oxide-derived nanocrystalline copper, Nature. 508 (2014) 504–507, https://doi.org/10.1038/nature13249.

[27] C.W. Li, M.W. Kanan, CO_2 reduction at low overpotential on Cu electrodes resulting from the reduction of thick Cu_2O films, J. Am. Chem. Soc. 134 (2012) 7231–7234, https://doi.org/10.1021/ja3010978.

[28] K.P. Kuhl, E.R. Cave, D.N. Abram, T.F. Jaramillo, New insights into the electrochemical reduction of carbon dioxide on metallic copper surfaces, Energy Environ. Sci. 5 (2012) 7050, https://doi.org/10.1039/c2ee21234j.

[29] E. Pérez-Gallent, G. Marcandalli, M.C. Figueiredo, F. Calle-Vallejo, M.T.M. Koper, Structure- and potential-dependent cation effects on CO reduction at copper single-crystal electrodes, J. Am. Chem. Soc. 139 (2017) 16412–16419, https://doi.org/10.1021/jacs.7b10142.

[30] J.E. Pander, D. Ren, Y. Huang, N.W.X. Loo, S.H.L. Hong, B.S. Yeo, Understanding the heterogeneous electrocatalytic reduction of carbon dioxide on oxide-derived catalysts, ChemElectroChem. 5 (2018) 219–237, https://doi.org/10.1002/celc.201701100.

[31] F.S. Roberts, K.P. Kuhl, A. Nilsson, Electroreduction of carbon monoxide over a copper nanocube catalyst: surface structure and pH dependence on selectivity, ChemCatChem. 8 (2016) 1119–1124, https://doi.org/10.1002/cctc.201501189.

[32] Y. Kwon, Y. Lum, E.L. Clark, J.W. Ager, A.T. Bell, CO_2 electroreduction with enhanced ethylene and ethanol selectivity by nanostructuring polycrystalline copper, ChemElectroChem. 3 (2016) 1012–1019, https://doi.org/10.1002/celc.201600068.

[33] C.S. Chen, A.D. Handoko, J.H. Wan, L. Ma, D. Ren, B.S. Yeo, Stable and selective electrochemical reduction of carbon dioxide to ethylene on copper mesocrystals, Catal. Sci. Technol. 5 (2015) 161–168, https://doi.org/10.1039/C4CY00906A.

[34] K.J.P. Schouten, E.P. Gallent, M.T.M. Koper, The electrochemical characterization of copper single-crystal electrodes in alkaline media, J. Electroanal. Chem. 699 (2013) 6–9, https://doi.org/10.1016/j.jelechem.2013.03.018.

[35] G. Bianchi, P. Longhi, Copper in sea-water, potential-pH diagrams, Corros. Sci. 13 (1973) 853–864, https://doi.org/10.1016/S0010-938X(73)80067-8.

[36] H. Liu, Y. Zhou, S.A. Kulinich, J.-J. Li, L.-L. Han, S.-Z. Qiao, X.-W. Du, Scalable synthesis of hollow Cu_2O nanocubes with unique optical properties via a simple hydrolysis-based approach, J. Mater. Chem. A 1 (2013) 302–307, https://doi.org/10.1039/C2TA00138A.

[37] Y. Hori, O. Koga, H. Yamazaki, T. Matsuo, Infrared spectroscopy of adsorbed CO and intermediate species in electrochemical reduction of CO_2 to hydrocarbons on a Cu electrode, Electrochim. Acta 40 (1995) 2617–2622, https://doi.org/10.1016/0013-4686(95)00239-B.

[38] A.S. Varela, M. Kroschel, T. Reier, P. Strasser, Controlling the selectivity of CO_2 electroreduction on copper: the effect of the electrolyte concentration and the

importance of the local pH, Catal. Today 260 (2016) 8–13, https://doi.org/10.1016/j.cattod.2015.06.009.

[39] D. Raciti, M. Mao, C. Wang, Mass transport modelling for the electroreduction of CO_2 on Cu nanowires, Nanotechnology. 29 (2018), 044001, https://doi.org/10.1088/1361-6528/aa9bd7.

[40] H.S. Jeon, J. Timoshenko, F. Scholten, I. Sinev, A. Herzog, F.T. Haase, B. Roldan Cuenya, Operando insight into the correlation between the structure and composition of CuZn nanoparticles and their selectivity for the electrochemical CO_2 reduction, J. Am. Chem. Soc. 141 (2019) 19879–19887, https://doi.org/10.1021/jacs.9b10709.

[41] D. Ren, B.S.-H. Ang, B.S. Yeo, Tuning the selectivity of carbon dioxide electroreduction toward ethanol on oxide-derived Cu x Zn catalysts, ACS Catal. 6 (2016) 8239–8247, https://doi.org/10.1021/acscatal.6b02162.

[42] S. Ikeda, S. Shiozaki, J. Susuki, K. Ito, H. Noda, Electroreduction of CO_2 using Cu/Zn Oxides Loaded Gas Diffusion Electrodes, 1998 225–230, https://doi.org/10.1016/S0167-2991(98)80748-9.

[43] H.-J. Yang, S.-Y. He, H.-L. Chen, H.-Y. Tuan, Monodisperse copper nanocubes: synthesis, self-assembly, and large-area dense-packed films, Chem. Mater. 26 (2014) 1785–1793, https://doi.org/10.1021/cm403098d.